

Half Metal Transition Driven by Doping Effects in Osmium Double Perovskite

Madhav P. Ghimire and Xiao Hu

*International Center for Materials Nanoarchitectonics (WPI-MANA),
National Institute for Materials Science, Tsukuba 305-0044, Japan*

(Dated: September 26, 2018)

Using the first-principles density functional approach, we investigate $\text{Ca}_2\text{FeOsO}_6$, a material of double perovskite structure synthesized recently. According to the calculations, $\text{Ca}_2\text{FeOsO}_6$ is a ferrimagnetic Mott-insulator influenced by the cooperative effect of spin-orbit coupling (SOC) and Coulomb interactions of Fe-3d and Os-5d electrons, as well as the crystal field. When Fe is replaced with Ni, the system exhibits half metallic (HM) states desirable for spintronic applications. In $[\text{Ca}_2\text{Fe}_{1-x}\text{Ni}_x\text{OsO}_6]_2$, HM ferrimagnetism is observed with $\mu_{\text{tot}} = 2\mu_B$ per unit cell for doping rate $x = 0.5$, whereas HM antiferromagnetism (HMAFM) with nearly zero spin magnetization in the unit cell for $x = 1$, respectively. It is emphasized that half metallicity is retained even with SOC effect due to the large exchange-splitting between spin-up and spin-down bands close to the Fermi level.

PACS numbers: 85.75.-d, 71.30.+h, 75.70.Tj, 71.15.Mb

I. INTRODUCTION

Double perovskite oxides have been widely investigated due to their interesting properties useful for spintronic applications^{1,2}. With the general formula $\text{A}_2\text{BB}'\text{O}_6$, A is usually an alkaline earth or rare-earth element, and B and B' are the transition metal elements, both of which are composed of edge-shared octahedra. Depending on the choice of B and B' cations, these compounds show a variety of electrical and magnetic properties, namely metallicity, half metallicity, insulator as well as ferromagnetism, ferrimagnetism, and antiferromagnetism¹. The discovery of room-temperature colossal magnetoresistance and half metallicity in Sr_2FeTO_6 (where T=Mo, Re)³⁻⁵, multiferroicity in $\text{Bi}_2\text{NiMnO}_6$ ⁶, magnetodielectricity in $\text{La}_2\text{NiMnO}_6$ ⁷, leads to intensive study in double perovskite materials. Recent researches have been devoted to understanding the electronic and magnetic properties of hybrid 3d-4d(5d) double perovskites which exhibit high spin polarization^{8,9} essential for device applications at room temperature.

Half metals (HMs) are a class of materials which are metallic in one spin channel, while insulating in the opposite spin channel due to the asymmetric band structure¹⁰⁻¹⁶. HMs allow spin polarized currents to flow without any external operation, and thus are very useful for spintronics applications. The total spin-moment per unit cell is quantized in units of Bohr magneton (μ_B) due to insulating state in one spin-channel. HMs have been identified in several groups of materials¹⁷⁻³⁰. Most of the experimentally available HMs are either ferromagnets (FM) or ferrimagnets (FiM) which give non-zero integer moments. It was noted that spin-polarized current can be hampered by stray fields which stabilize magnetic domains^{13,26}. This drawback can be overcome by HM antiferromagnets (HMAFM), a subclass of HMs characterized further by zero spin magnetization per unit cell^{11,12}. A number of materials with DP structures have been predicted as possible candidates of HMAFMs¹⁷⁻²².

Because of the recent success in synthesizing osmium oxides, osmates have been attracting significant interests yielding various unconventional phases. For instance, unusual superconductivity is observed in $\text{A}_2\text{Os}_2\text{O}_7$ (A=Cs, Rb and K)³¹. Magnetically driven metal-insulator transition is found in $\text{Cd}_2\text{Os}_2\text{O}_7$ ³² and NaOsO_3 ³³, and the ferroelectric-type structural transition has been discovered in metallic LiOsO_3 ³⁴. Among the double perovskites, magnetic insulating states in Sr_2MOsO_6 (where M=Cu, Ni)³⁵, Mott-insulating ferromagnetic state in $\text{Ba}_2\text{NaOsO}_6$ ³⁶, and half semi-metallic antiferromagnetism in $\text{Sr}_2\text{CrOsO}_6$ ³⁷ are a few examples that have been reported. A newly synthesized double perovskite material $\text{Ca}_2\text{FeOsO}_6$ comes into our attention which is reported to be a FiM insulator driven by lattice distortion with high Curie temperature (T_c)³⁸. The crystal has unique properties suitable for spintronic device applications: Fe and Os atoms carry on opposite spin magnetizations, and octahedra exhibit strong crystal distortion which may induce strong crystal field that helps in splitting the spin-up and spin-down bands. The origin of novel FiM state with T_c of 320K opens new possibility of realizing device applications at room temperature. We dope Ni atom having charge state +2 to replace Fe atom with charge state +3 to study its influence on the parent material $\text{Ca}_2\text{FeOsO}_6$.

We have performed first-principles density-functional calculations on $\text{Ca}_2\text{FeOsO}_6$ (CFOO). It is found that CFOO is a FiM Mott insulator with total angular momentum $\mu_{\text{tot}} = 4\mu_B$ per unit cell of $[\text{Ca}_2\text{FeOsO}_6]_2$. This material is interesting in the sense that the topmost valence states close to Fermi level (E_F) are exclusively spin-down bands contributed from 5d electrons of Os atoms, and the element Fe has no influence on the electronic state near E_F . Therefore, replacing Fe by 3d elements with more than five valence electrons one can make a fine control on charge and spin. Specifically, we consider the replacement of Fe atom by the Ni atom which shows interesting properties desirable in spintronics.

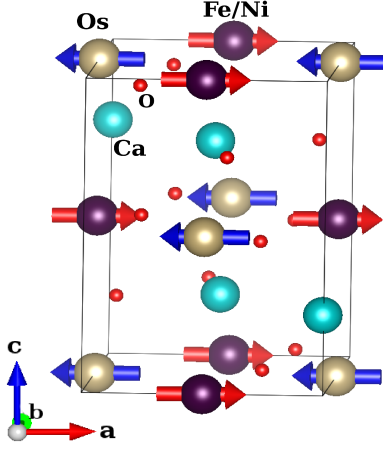


FIG. 1. Double perovskite structure of $[\text{Ca}_2\text{FeOsO}_6]_2$ and $[\text{Ca}_2\text{NiOsO}_6]_2$. The red (blue) arrows indicate the direction of Fe/Ni(Os) spins along the a direction which is the easy axis.

We find that the material $[\text{Ca}_2\text{Fe}_{1-x}\text{Ni}_x\text{OsO}_6]_2$ is HM-FiM with $\mu_{\text{tot}} = 2\mu_B$ at $x = 0.5$ and nearly compensated HMAFM with $\mu_{\text{tot}} = 0.3\mu_B$ at $x = 1$. The interplay among Coulomb repulsion, SOC and the crystal field plays an important role in this material.

The organization of this paper is as follows: Section II describes the details on crystal structure and methods. Section III presents the results on the parent material $[\text{Ca}_2\text{FeOsO}_6]_2$, while Sec. IV discusses the results on the possibility of obtaining half metallicity in the doped materials $[\text{Ca}_2\text{Fe}_{1-x}\text{Ni}_x\text{OsO}_6]_2$. Section V contains the discussions and the conclusions are drawn in Sec. VI.

II. CRYSTAL STRUCTURES AND METHODS

In the double perovskite $[\text{Ca}_2\text{FeOsO}_6]_2$ (CFOO), the transition metal Fe and Os occupy B and B' sites in an ordered way. The crystal structure of CFOO shown in Fig. 1 falls in the space group $P2_1/n$ with monoclinic-distortion. It has structural distortions due to the tilting and rotation of the two corner-sharing FeO_6 and OsO_6 octahedra.

The electronic and magnetic structure calculations were performed within density-functional theory (DFT) by using the full-potential linearized augmented plane wave plus local orbital method implemented in the WIEN2k code³⁹. The atomic sphere radii R_{MT} were 2.17, 1.99, 1.99, 2.0 and 1.64 Bohr for Ca, Fe, Ni, Os and O respectively. A set of 1000 k -points were used in the full Brillouin zone. The standard generalized-gradient approximation (GGA) exchange-correlation potential within the PBE-scheme⁴⁰ were used with Coulomb interaction U of 5eV for Fe (Ni) and 1.5eV for Os, respectively^{41,42}. Spin-orbit coupling is considered via a second variational step using the scalar-relativistic eigen-

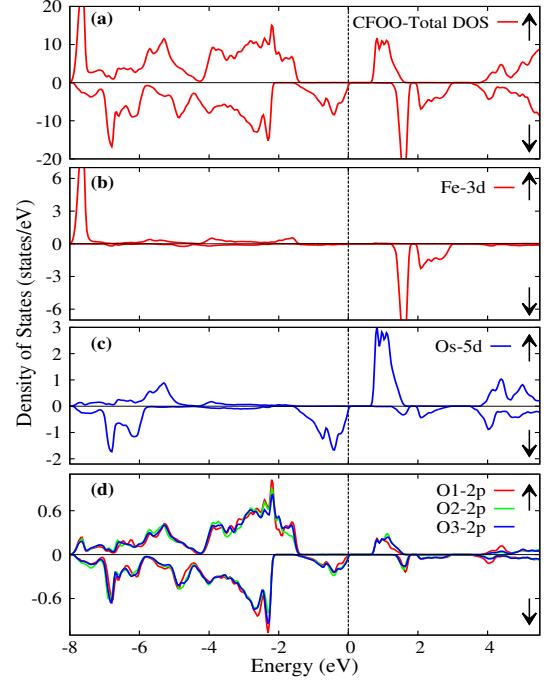


FIG. 2. Density of states for $[\text{Ca}_2\text{FeOsO}_6]_2$ in spin-up (\uparrow) and spin-down (\downarrow) channels: (a) total, (b) Fe-3d states, (c) Os-5d states and (d) three inequivalent oxygen-2p states.

functions as basis⁴³. We checked different magnetic configurations of Fe, Ni and Os sites and found that the FiM structure shown in Fig. 1 is the ground state consistent with the experiments^{38,44}.

III. PARENT MATERIAL $[\text{Ca}_2\text{FeOsO}_6]_2$

In CFOO, the transition element Fe nominally takes the charge state +3 with $3d^5$ configuration. These five valence electrons occupy the t_{2g} and e_g orbitals resulting to a high-spin (HS) state of Fe. On the other hand, Os takes the charge state +5 with $5d^3$ configuration, where three valence electrons occupy the t_{2g} orbitals giving rise to HS state.

To gain insight into the electronic properties of CFOO the spin-resolved total and partial density of states (DOS) in spin-up and spin-down channels are shown in Fig. 2. According to first-principles calculations, there is an energy gap of $\sim 0.8\text{eV}$ at E_F , indicating clearly that CFOO is a Mott insulator. This result is consistent with the recent experimental report of the insulating state in CFOO³⁸. Fe-3d (i.e., t_{2g}^3 and e_g^2) states in spin-up channel are fully occupied and remain deep in the valence region, whereas the states in spin-down channel lie in the conduction region. Unlike Fe, Os-5d (i.e., t_{2g}^3) states are located in the conduction region with a broad peak for spin-up channel indicating the empty states, whereas in spin-down channel they occupy the topmost valence

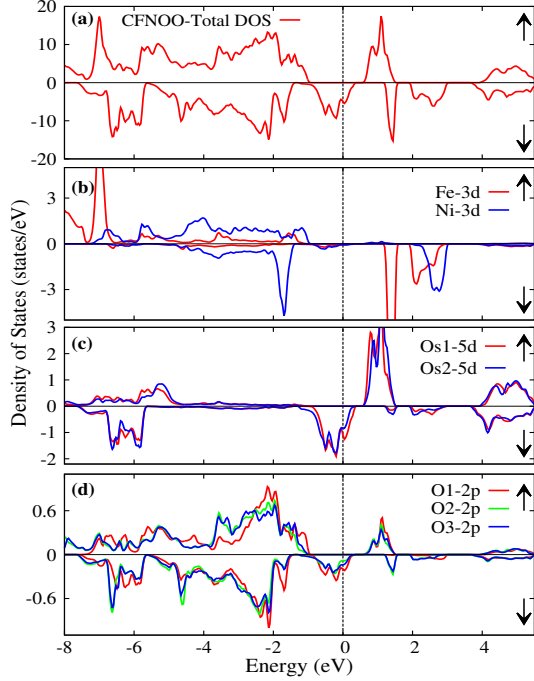


FIG. 3. Density of states for $[\text{Ca}_2\text{Fe}_{0.5}\text{Ni}_{0.5}\text{OsO}_6]_2$ in spin-up (\uparrow) and spin-down (\downarrow) channels: (a) total, (b) Fe-3d/Ni-3d states, (c) Os-5d states, and (d) three inequivalent oxygen-2p states

bands below E_F . As observed in Fig. 2(d), oxygen bands below E_F in both spin-channels hybridize with the Fe-3d and Os-5d states. This is caused due to octahedral distortions, where three sorts of oxygen positions with different Fe(Os)-O bond-lengths appear.

The magnetic property of CFOO is of particular interests. At the ground state obtained from first-principles calculations, Fe couples antiferromagnetically with Os. The calculated total moment (μ_{tot}) is $4.0\mu_B$ per unit cell (see Table I). In an ionic picture, each Fe ion carries moment $+5\mu_B$ while Os ion carries $-3\mu_B$, giving rise to $\mu_{\text{tot}} = 2 \times (+5\mu_B) + 2 \times (-3\mu_B) = 4\mu_B$ in $[\text{Ca}_2\text{FeOsO}_6]_2$, consistent with the first-principles calculations.

IV. DOPED MATERIALS $[\text{Ca}_2\text{Fe}_{1-x}\text{Ni}_x\text{OsO}_6]_2$

The above properties makes CFOO a promising candidate for exploring possible HM states with fine control on charge and magnetic moments. HM states can be achieved in CFOO by doping 3d transition metals having valence electron larger than five. To be specific, we consider the B-site modification by replacing one Fe atom with Ni in $[\text{Ca}_2\text{FeOsO}_6]_2$, an element having charge state +2 with $3d^8$ configuration. Out of eight valence electrons five occupy the t_{2g} and e_g orbits of spin-up channel while the remaining three occupy the t_{2g} orbits in spin-down channel giving rise to a moment of $2\mu_B$ per Ni atom.

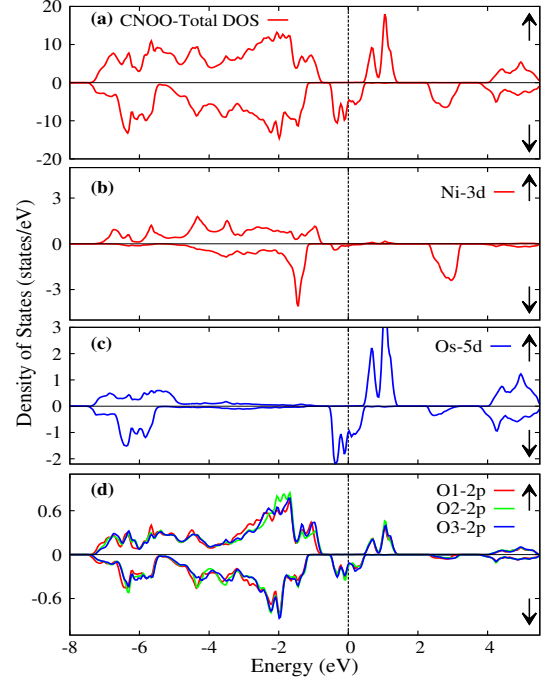


FIG. 4. Density of states for $[\text{Ca}_2\text{NiOsO}_6]_2$ in spin-up (\uparrow) and spin-down (\downarrow) channels: (a) total, (b) Ni-3d states, (c) Os-5d states and (d) three inequivalent oxygen-2p states.

Ni doping corresponds to addition of three extra electrons to the system. Since the charge states of Fe(+3) and Ni(+2) differ from each other, the Os atom interacting with Fe has a charge state +5 and $5d^3$ configuration while the other one interacting with Ni has +6 charge state and $5d^2$ configuration, to maintain charge neutral in the system. Thus, Ni doping will influence the system by (i) shifting the Os bands towards the conduction region, and (ii) compensating magnetic moment by $2\mu_B$ per each Fe replacement. In this way, one can modify the material to design the desired HMFIM and HMAFM.

We perform first-principles calculations to check the above idea for replacement rate $x = 0.5$ in $[\text{Ca}_2\text{Fe}_{1-x}\text{Ni}_x\text{OsO}_6]_2$. As shown in Fig. 3, Fe-3d states in spin-up channel are fully occupied lying deep in the valence region, whereas for spin-down channel they remain in the conduction region. The Ni-3d bands are also occupied in spin-up channel while the spin-down bands are partially occupied with a localized peak at -1.8eV below E_F . The remaining bands appear in the conduction region. This happens because five out of eight d electrons from Ni occupy the spin-up channel and the three remaining electrons go to spin-down channel to fill the t_{2g} orbits. Due to repulsive interaction from spin-down Ni-3d electrons, Os- t_{2g} electrons which were originally lying at the topmost valence region in the parent material (see Fig. 2) shift towards the conduction region crossing E_F (see Fig. 5(b)). As the results, the Os- t_{2g} states crossing E_F form a continuous band and give rise to metallic state

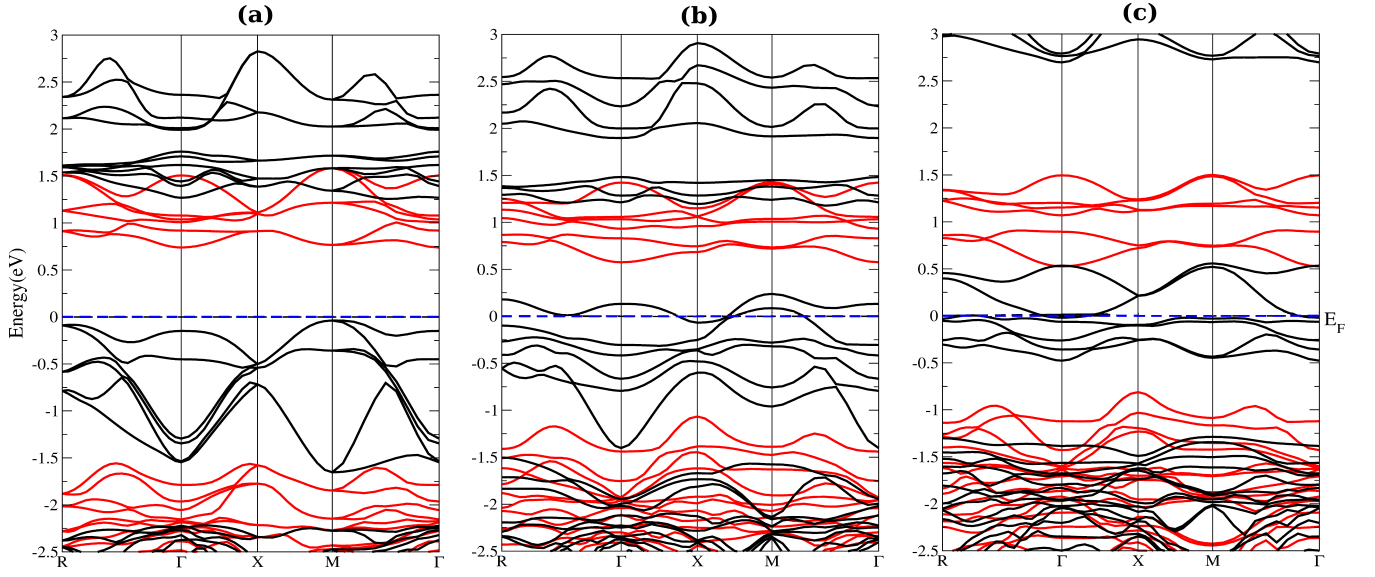


FIG. 5. Band structures for doping rate (a) $x = 0$, (b) $x = 0.5$ and (c) $x = 1$ in $[\text{Ca}_2\text{Fe}_{1-x}\text{Ni}_x\text{OsO}_6]_2$ for spin-up (red) and spin-down (black) channels.

for spin-down channel. Hence, with spin-up channel insulating and spin-down channel metallic, the material is a half metal.

Let us now focus to the most interesting case of replacement rate $x = 1$, where both Fe atoms are replaced by Ni atoms within unit-cell. From the first principles calculations the FiM ground state is $\sim 135\text{meV}$ less than the first excited AFM state. Due to the presence of Ni atom alone on the B-site, Os atom fully attains the charge state $+6$ with $5d^2$ configuration unlike in the parent material $[\text{Ca}_2\text{FeOsO}_6]_2$. For Ni of d^8 , three t_{2g} and two e_g orbitals in spin-up channel and three t_{2g} orbitals in spin-down channel are occupied. For Os of d^2 , only two t_{2g} orbitals in spin-down channel are occupied. The system is then expected to favor half metallicity with full compensation of total moment. As revealed by the DOS shown in Fig. 4, Ni-3d states are fully occupied in spin-up channel by five electrons and the remaining electrons go to occupy the t_{2g} orbitals in spin-down channel. This is evident with the occupation of Ni-3d states in the valence region with a localized peak at -1.6eV below E_F . The unoccupied e_g band appears far in the conduction region. The Os-5d states are almost empty in spin-up channel but has partial occupation with a band crossing E_F in spin-down channel. This is caused mainly by the spin-down electrons of Ni which push the Os- t_{2g} states up towards the conduction region. Thus, two of the t_{2g} states of Os atom remain in the valence region while the unoccupied state moves to the conduction region crossing E_F (see also Fig. 5(c)). Due to crystal distortion, gap could not open-up among the t_{2g} states of Os atom which results in metallic state in spin-down channel. Oxygen 2p states are found to hybridize strongly with Os-5d states near E_F in both spin channels. Thus, with spin-up channel insu-

TABLE I. Moments per atom of Fe[Ni] and Os, one set of three in-equivalent oxygen atoms and unit cell (μ_{tot}) for replacement rate x in $[\text{Ca}_2\text{Fe}_{1-x}\text{Ni}_x\text{OsO}_6]_2$ from first-principles calculations. The unit of moments is the Bohr magneton μ_B . The contributions from individual atoms are within muffintins while the total angular moment includes those from interstitial regime.

x	Fe [Ni]	Os	O	μ_{tot}
0	4.13	-1.6	-0.11	4.0
0.5	4.13 [1.68]	-1.36	-0.15	2.0
1	[1.68]	-1.09	-0.14	0.3

lating and spin-down channel metallic, the system turns to a HM as clearly seen in Fig. 4.

As summarized in Table I, two replaced Fe atoms take away $\mu \simeq 2\mu_B$, and the charge transfer in two Os atoms associated on doping reduces $\mu \simeq 2\mu_B$ further, resulting in compensation of total moment to zero. The results obtained by first-principles calculations are consistent with the ionic picture. These features can also be seen from the spin-density isosurface plot in Fig. 5(b). With the zero total moment and HM property, the material $[\text{Ca}_2\text{NiOsO}_6]_2$ should be a HMAFM. However, SOC induces an orbital moment of $\sim 0.17\mu_B$ across Os resulting in the total moment of $0.3\mu_B$ per unit cell. Hence the material may be called a nearly compensated half metal.

V. DISCUSSIONS

In order to give a clear picture on how doping changes the electronic structure for $x = 0, 0.5$ and 1 in $[\text{Ca}_2\text{Fe}_{1-x}\text{Ni}_x\text{OsO}_6]_2$, band structure plots are shown in

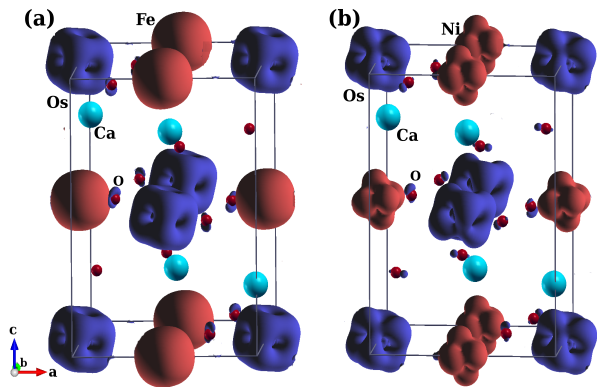


FIG. 6. Isosurface of spin magnetization density at $\pm 0.21 e/\text{\AA}^3$ with red (blue) for spin up (down): (a) parent material $[\text{Ca}_2\text{FeOsO}_6]_2$, (b) material with full Fe replacement $[\text{Ca}_2\text{NiOsO}_6]_2$.

Fig. 5. It should be noted that six bands lying in the top-most valence region below E_F in the parent material (i.e. $x = 0$) are the t_{2g} bands contributed by two Os atoms in spin-down channel (see Fig. 5(a)). It is interesting to note that half replacement of Fe by Ni corresponds to shifting of one of the t_{2g} band towards the conduction region. As clearly observed for $x = 0.5$, five out of six of the t_{2g} bands are occupied while the remaining one band moves to the conduction region. As similar case is observed for $x = 1$ where four t_{2g} bands remain below E_F while the two bands go to conduction region.

In the present materials, SOC is crucially important due to the presence of heavy elements such as Os. The orbital moments obtained from first-principles calculations for Os ($0.1 \sim 0.2\mu_B$) are in accordance with the Hund's third rule⁴⁵. SOC reduces the band gap by $\sim 0.1\text{eV}$ through the broadening of Os-5d states in the parent material. SOC induces the total moment of $0.3\mu_B$ per unit cell for $[\text{Ca}_2\text{NiOsO}_6]_2$ which is in reasonable agreement with the experiment⁴⁴.

Charge-transfer effect⁴⁶ is prominent between Os and oxygen via t_{2g} and p states in the parent material. Therefore, oxygens get spin-polarized in parallel with the Os ions, consistent with the isosurface plot shown in Fig. 6(a). The isosurface of Fe-3d states are spherical due to occupation of all the d orbitals in spin-up channel.

Os on the other hand shows the t_{2g} characters. The full replacement of Fe with Ni shows an active e_g like orbitals (see Fig. 6(b)). The size of the Os- t_{2g} isosurface reduces in the doped material due to one electron less than in the parent material.

First-principles calculations on magnetic anisotropy energy indicates a axis of the crystal as the easy axis (see Fig. 1) with anisotropy energy of $\sim 2\text{meV}$ and $\sim 4\text{meV}$ per unit cell for $\text{Ca}_2\text{FeOsO}_6$ and $\text{Ca}_2\text{NiOsO}_6$ respectively.

Robustness of half metallicity is checked for doping rate $x = 1$ by considering the (i) antisite disorder and (ii) surface effects with a vacuum of 20\AA along 001. We have confirmed that the HM state remains stable in both configurations.

In the present work, HMAFM and HMFm have been derived from the same parent material. Thus, using them in an integrated system, one can construct a useful device for spintronics applications without suffering from the problem of lattice mismatching.

VI. CONCLUSIONS

Based on the first-principles density functional approach, we propose material tailoring on a Mott insulator $[\text{Ca}_2\text{FeOsO}_6]_2$ with double perovskite structure exploiting the cooperative effect from Coulomb interaction, spin-orbit coupling and the crystal field. It is demonstrated that replacing Fe by Ni, one can achieve several half metals. Especially, $[\text{Ca}_2\text{NiOsO}_6]_2$ is found to be a nearly compensated half metals, which is ideal for spintronic applications. It is emphasized that the large exchange splitting between spin-up and spin-down bands at the Fermi level retains the half metallicity even in presence of strong spin-orbit coupling.

ACKNOWLEDGMENTS

The authors thank K. Yamaura for providing the crystal information of the parent material. This work was supported by WPI Initiative on Materials Nanoarchitectonics, MEXT, Japan.

- ¹ M. T. Anderson, K. B. Greenwood, G. A. Taylor, and K. R. Poeppelmeier, Prog. Solid. State Chem. **22**, 197 (1993).
- ² S. A. Wolf, D. D. Awschalom, R. A. Buhrman, J. M. Daughton, S. von Molnar, M. L. Roukes, A. Y. Chtchelkanova, and D. M. Treger, Science **294**, 1488 (2001).
- ³ K.-I. Kobayashi, T. Kimura, H. Sawada, K. Terakura, and Y. Tokura, Nature (London) **395**, 677 (1998).
- ⁴ D. D. Sarma, P. Mahadevan, T. Saha-Dasgupta, S. Ray, and A. Kumar, Phys. Rev. Lett. **85**, 2549 (2000).
- ⁵ Y. Tokura, Rep. Prog. Phys. **69**, 797 (2006).

- ⁶ Y. Shimakawa, M. Azuma, and N. Ichikawa, Materials **4**, 153 (2011).
- ⁷ N. S. Rogado, J. Li, A. W. Sleight, and M. A. Subramanian, Adv. Mater. **17**, 2225 (2005).
- ⁸ O. N. Meetei, O. Erten, A. Mukherjee, M. Randeria, N. Trivedi, and P. Woodward, Phys. Rev. B **87**, 165104 (2013).
- ⁹ O. Erten, O. N. Meetei, A. Mukherjee, M. Randeria, N. Trivedi, and P. Woodward, Phys. Rev. B **87**, 165105 (2013).

- ¹⁰ R. A. de Groot, F. M. Mueller, P. G. van Engen, and K. H. J. Buschow, Phys. Rev. Lett. **50**, 2024 (1983).
- ¹¹ H. van Leuken, and R. A. de Groot, Phys. Rev. Lett. **74**, 1171 (1995).
- ¹² X. Hu, Adv. Mater. **24**, 294 (2012).
- ¹³ H. Kurt, K. Rode, P. Stamenov, M. Venkatesan, Y.-C. Lau, E. Fonda, and J. M. D. Coey, Phys. Rev. Lett. **112**, 027201 (2014).
- ¹⁴ W. E. Pickett, and J. S. Moodera, Physics Today **54**, 39 (2001).
- ¹⁵ C. Felser, G. H. Fecher, and B. Balke, Angew. Chem. Int. Ed. **46**, 668 (2007).
- ¹⁶ M. I. Katsnelson, Y. Yu. Irkhin, L. Chioncel, A. I. Liechtenstein, and R. A. de Groot, Rev. Mod. Phys. **80**, 315 (2008).
- ¹⁷ W. E. Pickett, Phys. Rev. B **57**, 10613 (1998).
- ¹⁸ J. H. Park, S. K. Kwon, and B. I. Min, Phys. Rev. B **65**, 174401 (2002).
- ¹⁹ M. Uehara, M. Yamada, and Y. Kimishima, Solid State Commun. **129**, 385 (2004).
- ²⁰ M. S. Park and B. I. Min, Phys. Rev. B **71**, 052405 (2005).
- ²¹ Y. K. Wang and G. Y. Guo, Phys. Rev. B **73**, 064424 (2006).
- ²² V. Pardo and W. E. Pickett, Phys. Rev. B **80**, 054415 (2009).
- ²³ X. Wan, M. Kohno, and X. Hu, Phys. Rev. Lett. **94**, 087205 (2005); *ibid.* **95**, 146602 (2005).
- ²⁴ H. Akai, and M. Ogura, Phys. Rev. Lett. **97**, 026401 (2006).
- ²⁵ Y.-M. Nie, and X. Hu, Phys. Rev. Lett. **100**, 117203 (2008).
- ²⁶ G. M. Müller, J. Walowski, M. Djordjevic, G.-X. Miao, A. Gupta, A. V. Ramos, K. Gehrke, V. Moshnyaga, K. Samwer, J. Schmalhorst, A. Thomas, A. Hütten, G. Reiss, J. S. Moodera, and M. Münzenberg, Nat. Mater. **8**, 56 (2009).
- ²⁷ S.-J. Hu, and X. Hu, J. Phys. Chem. C **114**, 11614 (2010).
- ²⁸ M. P. Ghimire, Sandeep, T. P. Sinha, and R. K. Thapa, J. Alloys Compd. **509**, 9742 (2011).
- ²⁹ M. P. Ghimire, L.-H. Wu, and X. Hu, e-print arXiv:1407.3408.
- ³⁰ M. P. Ghimire, R. K. Thapa, D. P. Rai, T. P. Sinha, and X. Hu, e-print arXiv:1408.1216.
- ³¹ Z. Hiroi, J. Yamaura, and K. Hattori, J. Phys. Soc. Jpn **81**, 011012 (2012).
- ³² J. Yamaura, K. Ohgushi, H. Ohsumi, T. Hasegawa, I. Yamauchi, K. Sugimoto, S. Takeshita, A. Tokuda, M. Takata, M. Udagawa, M. Takigawa, H. Harima, T. Arima, and Z. Hiroi, Phys. Rev. Lett. **108**, 247205 (2012).
- ³³ S. Calder, V. O. Garlea, D. F. McMorrow, M. D. Lumsden, M. B. Stone, J. C. Lang, J. W. Kim, J. A. Schlueter, Y. G. Shi, K. Yamaura, Y. S. Sun, Y. Tsujimoto, and A. D. Christianson, Phys. Rev. Lett. **108**, 257209 (2012).
- ³⁴ Y. G. Shi, Y. F. Guo, X. Wang, A. J. Princep, D. Khalyavin, P. Manuel, Y. Michiue, A. Sato, T. Tsuda, S. Yu, M. Arai, Y. Shirako, M. Akaogi, N. L. Wang, K. Yamaura, A. T. Boothroyd, Nat. Mater. **12**, 1023 (2013).
- ³⁵ C. Tian, A. C. Wibowo, H.-C. zur Loye, and M.-H. Whangbo, Inorg. Chem. **50**, 4142 (2011).
- ³⁶ H. J. Xiang, and M. H. Whangbo, Phys. Rev. B **75**, 052407 (2007).
- ³⁷ K.-W. Lee, and W. E. Pickett, Phys. Rev. B **77**, 115101 (2008).
- ³⁸ H. L. Feng, M. Arai, Y. Matsushita, Y. Tsujimoto, Y. Guo, C. I. Sathish, X. Wang, Y. H. Yuan, M. Tanaka, and K. Yamaura, J. Am. Chem. Soc. **136**, 3326 (2014).
- ³⁹ P. Blaha, K. Schwarz, G. K. H. Madsen, D. Kvasnicka, and J. Luitz, *WIEN2k, An Augmented Plane Wave + Local Orbitals Program for Calculating Crystal Properties* (Technische Universität Wien, Vienna, Austria, 2001), ISBN 3-9501031-1-2.
- ⁴⁰ J. P. Perdew, K. Burke, and M. Ernzerhof, Phys. Rev. Lett. **77**, 3865 (1996).
- ⁴¹ A. I. Liechtenstein, V. I. Anisimov, and J. Zaanen, Phys. Rev. B **52**, R5467 (1995); V. I. Anisimov, F. Aryasetiawan, and A. I. Liechtenstein, J. Phys.: Condens. Matter **9**, 767 (1997).
- ⁴² The obtained results for the present materials are robust with $U = 2 - 8\text{eV}$ for Fe(Ni) and $0.5 - 2.75\text{eV}$ for Os, respectively⁴¹.
- ⁴³ J. Kuneš, P. Novák, R. Schmid, P. Blaha, and K. Schwarz, Phys. Rev. B **64**, 153102 (2001).
- ⁴⁴ R. Macquart, S.-J. Kim, W. R. Gemmill, J. K. Stalick, Y. Lee, T. Vogt, and H.-C. zur Loye, Inorg. Chem. **44**, 9676 (2005).
- ⁴⁵ C. Kittel, *Introduction to Solid State Physics*, 8th ed. (Wiley, Hoboken, 2005).
- ⁴⁶ J. Zaanen, G. A. Sawatzky, and J. W. Allen, Phys. Rev. Lett. **55**, 418 (1985).